Cosmic Ray Sun Shadow in Soudan 2 Underground Muon Flux

**W.W.M. Allison,[3], G.J. Alner[4], D.S. Ayres[1], W.L. Barrett,[6], C. Bode,[2], P.M. Border[2], C.B. Brooks[3],
J.H. Cobb[3], R.J. Cotton[4], H. Courant[2], D.M. Demuth[2], T.H. Fields[1], H.R. Gallagher[3],
C. Garcia-Garcia[4], M.C. Goodman[1], R. Gran[2], T. Joffe-Minor[1], T. Kafka[5], S.M.S. Kasahara[2],
W. Leeson[5], P.J. Litchfield[4], N.P. Longley[2], W.A. Mann[5], M.L. Marshak[2], R.H. Milburn[5],
W.H. Miller[2], L. Mualem[2], A. Napier[5], W.P. Oliver[5], G.F. Pearce[4], E.A. Peterson[2], D.A. Petyt[4],
L.E. Price[1], K. Ruddick[2], M. Sanchez[5], J. Schneps[5], M.H. Schub[2], R. Seidlein[1], A. Stassinakis[3],
J.L. Thron[1], V. Vassiliev[2], G. Villaume[2], S. Wakely[2], N. West[3], D. Wall[5]**
(The Soudan 2 Collaboration)
[1]*Argonne National Laboratory, Argonne, IL 60439, USA*
[2]*University of Minnesota, Minneapolis, MN 55455, USA*
[3]*Department of Physics, University of Oxford, Oxford OX1 3RH, UK*
[4]*Rutherford Appleton Laboratory, Chilton, Didcot, Oxfordshire OX11 0QX, UK*
[5]*Tufts University, Medford MA 02155, USA*
[6]*Western Washington University, Bellingham, WA 98225, USA*

Abstract

The absorption of cosmic rays by the sun produces a shadow at the earth. The angular offset and broadening of the shadow are determined by the magnitude and structure of the interplanetary magnetic field (IPMF) in the inner solar system. We report the first measurement of the solar cosmic ray shadow by detection of deep underground muon flux in observations made during the entire ten-year interval 1989 to 1998. The sun shadow varies significantly during this time, with a 3.3σ shadow observed during the years 1995 to 1998.

1 Introduction

The interplanetary magnetic field (IPMF) is produced by the trapping of the sun's magnetic field in the solar wind. The Archimedean spiral model for the IPMF, first described by Parker (1963), suggests that away from the immediate vicinity of the sun, the IPMF field lines lie preferentially in the region of the solar equatorial plane (nearly the ecliptic plane), varying in direction from radial near the sun to $\approx 40°$ from radial at 1 AU. This curvature is caused caused by the sun's rotation. Although the IPMF has been studied for many years, most measurements at ≤ 1 AU are from satellite data recorded about 1 percent of the distance from the earth to the sun.

The entire IPMF in the inner region of the ecliptic plane ($0 \leq r \leq 1$ AU) can be measured in the aggregate sense by measuring the cosmic ray shadow of the sun. This measurement may be used, in conjunction with satellite magnetic field measurements near the earth, to test the validity of field models. Several such measurements have been made using surface air-shower arrays. For many of these measurements, however, the combination of poor detector resolution, high cosmic ray energies and short observing times makes clear inferences about the IPMF difficult (Alexandreas, 1991; Borione, 1994; Merck, 1996). The Tibet Air Shower Array is the only detector to directly relate cosmic ray shadow characteristics to IPMF variability (Amenomori, 1996).

The Soudan 2 deep underground, iron, tracking calorimeter provides a new mode–deep underground muons rather than air showers–for measuring the cosmic ray shadow of the sun. This detector has been described in detail elsewhere (Allison, 1996). Most important for this discussion is that Soudan 2 has observed a clear cosmic ray shadow of the moon (Cobb, 1999) with a statistical significance of 5σ and an apparent Gaussian point spread function with $\sigma_r = 0.29°$ (including angular dispersion due to detector resolution and alignment, geomagnetic deflection, shower and muon production and the $0.26°$ radius of the moon). Differences between this lunar shadow and the simultaneously observed solar shadow may be ascribed to the magnetic field in the sun's immediate vicinity and the IPMF.

The expected offset and broadening of the solar cosmic ray shadow can be estimated from the satellite magnetic field measurements using the Parker model. Because the field lines radiate out from the sun and are only constrained to the solar equatorial (or ecliptic) planes by a $\sin\theta$ factor, flux conservation requires that the radial field B_r (the major field component between the sun and the earth) varies approximately as $1/r^2$, where r is the distance from the sun. Using geocentric solar ecliptic coordinates (GSE), in the ecliptic plane near the sun, B_x dominates (x points from the earth to the sun) and B_z and B_y are small (z points normal to the ecliptic, positive in the direction closer to the earth's north pole; y completes a right-handed, Cartesian coordinate system). The Archimedean spiral model ($\theta = ar$, where a is a constant), implies that for small θ ($\theta \approx \sin\theta$), $\frac{B_y}{|B|}$, increases proportional to r. Thus, B_y varies as $1/r$ between the sun and the earth. B_z in the ecliptic plane remains a small fraction of B_x out to large distances, with a radial dependence likely between $1/r$ and $1/r^2$.

In the impulse approximation, $\theta = \frac{0.3 \int B_t dx}{p}$, where θ is the deflection angle in mr, p is the particle momentum in TeV/c, B_t is the magnetic field transverse to the particle trajectory in T and x is the path length in m. The sun-earth distance is 1.5×10^{11} m or ≈ 215 solar radii. The shadow offset is determined by the mean tranverse field and the mean momentum. The shadow broadening is determined by the mean and rms transverse fields, the mean momentum and the rms momentum dispersion. The average daily mean (rms daily mean) values for B_y and B_z measured by satellites for the entire 1989-1998 interval are $B_y = -0.11$ nT (3.43 nT) and $B_z = 0.11$ nT (1.85 nT) (OmniWeb, 1999). Monte Carlo studies suggest that the mean momentum for cosmic ray primaries from the direction of the sun producing muons at Soudan 2 is 20 TeV/c and the rms momentum dispersion is of similar magnitude. Table 1 below shows the expected offset and broadening of the solar cosmic ray shadow in the north-south (due to B_y) and east-west (due to B_z) planes, using a $1/r$ dependence for B_y and both a $1/r$ and $1/r^2$ dependence for B_z. The table separately shows the expected broadening due to magnetic field variation and momentum dispersion, although these two effects are of approximately equal magnitude under the assumptions that $\Delta p \approx p$ and $\Delta B \approx B$. The rightmost column shows the expected combined effect calculated as a quadrature. The calculations used to determine the table entries are as follows: Assume B_{obs} is the y or z component of B measured near the earth. For a $1/r$ dependence, $p\theta = B_{obs} \times 1.5 \times 10^{11} m \times 0.3 \times f$, where f is approximately $(\ln 215 - \ln 10) = 2.4$, since 215 is the number of solar radii in 1 AU and 10 is the approximate distance from the sun in solar radii at which the Parker model becomes valid. For a $1/r^2$ dependence, $p\theta = B_{obs} \times 3.2 \times 10^{12} m \times (0.3)$, a quantity which is 9 times larger than the 1/r value. It is clear from the values in Table 1 that observation of a shadow distinguishes between $1/r$ and $1/r^2$ dependences for B_z. Even for $1/r$ dependences, observation of a shadow in the Soudan 2 data is considerably more probable during intervals in which the magnetic field is smaller than its average value over the 1989-1998 decade.

Table 1. Offset and broadening angles expected for solar shadow based on IPMF measurements and the Parker model.

	Offset Angle	Broadening Angle B Variation	Broadening Angle p Variation	Broadening Angle Overall
	(Degrees)	(Degrees)	(Degrees)	(Degrees)
B_y (1/r dependence)	0.08	1.1	1.1	1.6
B_z (1/r dependence)	0.08	0.57	0.57	0.8
B_z ($1/r^2$ dependence	0.72	5.1	5.1	7.2

2 Data Collection and Analysis

The data sample, collection procedure and muon track analysis used for the sun shadow data are similar to those used for a moon shadow analysis. The background, that is the number of events expected in the absence of a shadow, has been estimated differently. The background algorithm used for the sun shadow is to generate

a 100 times real sample ensemble of pseudo-events, using random combinations of arrival times and arrival directions in detector coordinates of real events. The pseudo-events are then analyzed in the same way as real events and pseudo-event distributions divided by 100 are then compared to real event distributions.

Fig. 1(a) shows a plot of the angular density of muons, $(1/\pi)(dN_\mu/d\theta^2)$ vs. θ, the angular distance between the muon direction and the calculated position of the center of the sun. The background distribution (not shown) indicates that in the absence of a shadow this plot should be flat. The real events, however, show a deficit at small angles. This deficit is both shallower and wider than the Soudan 2 muon shadow for the moon observed during the same interval, as is expected because of the effect of the IPMF. The significance of the shadow is tested by fitting the real event distribution to the form

$$\frac{dN_\mu}{d\theta^2} = \pi\lambda(1 - \pi(R_s^2/2\sigma^2)exp(-\theta^2/2\sigma^2)) \tag{1}$$

where the unshadowed density $\lambda = 526.8 \pm 0.3$ is determined from the background and R_s (the apparent radius of the sun) and σ are fitted parameters. σ folds together all offset and broadening effects including deflections due to the solar magnetic field and the IPMF, the finite angular size of the sun, geomagnetic deflections, shower and muon production effects, multiple Coulomb scattering and the the angular resolution and directional alignment of the detector. The best fit parameters for the entire data sample are $R_s = 0.174° \pm 0.026°$–significantly less than the geometric size of the sun–and $\sigma = 0.59°^{+0.17°}_{-0.10°}$–significantly more than the detector angular resolution. The chance probability for the improvement in the χ^2 from 74.2 (80 df) for no fit to 63.5 (78 df) with a two-parameter fit is 4.8×10^{-3}.

The results of a two-dimensional analysis for the same data sample is shown in Fig. 1(b). The center of the sun is at the center of the plot. The horizontal and vertical axes are displacements in degrees measured parallel and perpendicular to the ecliptic plane using $0.02°$ by $0.02°$ bins. The bin contents for both real and background events have then been smoothed with a $\sigma = 0.59°$ kernel. The plot in Fig. 1(b) is a contour map of z in units of standard deviations of the difference between real and background event distributions. The sun shadow is clearly visible, with a maximum depth of $z = -3.94$ at $0.18°$ ecliptic longitude and $-0.44°$ ecliptic latitude from the sun.

The 10-year data collection interval spans much of an 11-year solar cycle during which solar magnetic field and sunspot activity peaked in 1989-1991 and was at a minimal level in 1996. Maps similar to the one in Fig. 1(b) are shown in Fig. 1(c) for 1989 to 1994 and Fig 1(d) for 1995 to 1998, each with approximately half of the total number of events. The average daily satellite-measured IPMF (sunspot number) was 6.7 nT (104) for the former interval and 4.8 nT (28) for the latter one. For the interval of high field and sunspot activity, Fig. 1(c) shows no evidence for a distinct shadow. The shadow is clearly seen in Fig. 1(d), however, for the years with low field and sunspot activity. An analysis similar to the one similar to the one described above for Fig. 1(a) yields a chance probability for the shadow in Fig. 1(d) of 5.2×10^{-4} or 3.3σ as a one-tailed Gaussian probability. For Fig. 1(d), $R_s = 0.21° \pm 0.03°$, again less than the geometric size of the sun.

3   Conclusions

We have observed the shadow of the sun in deep underground muons with a chance probability of 4.8×10^{-3} during the years 1989 to 1998. The existence of a shadow implies that the IPMF normal to the ecliptic plane varies no more steeply than $1/r$, where r is the distance from the sun. An examination of approximately half of the data, that collected during 1989-1994, an interval of high magnetic field and sunspot activity, shows no evidence for a distinct shadow. The other half of the data sample collected during 1995-1998 shows a clear shadow with a chance probability equivalent to 3.3σ.

References

Alexandreas, D.E., *et al.*, 1991 Phys. Rev. **D43**, 1735.
Allison, W.W.M., *et al.*, 1996 Nucl. Inst. and Meth. **A376**, 377 and **A381**, 385.

Amenomori, M., *et al.*, 1996 Astrophys. J. **464**, 954.

Borione, A., *et al.*, 1994 Phys. Rev. **D49**, 1171.

Cobb, J.H., *et al.*, 1999 ICRC Paper SH 3.2.42.

Merck, M., *et al.*, 1996 Astropart. Phys. **5**, 379.

OmniWeb, 1999 Natl. Space Sci. Data Center, NASA Goddard Space Flight Center, Greenbelt MD, USA.

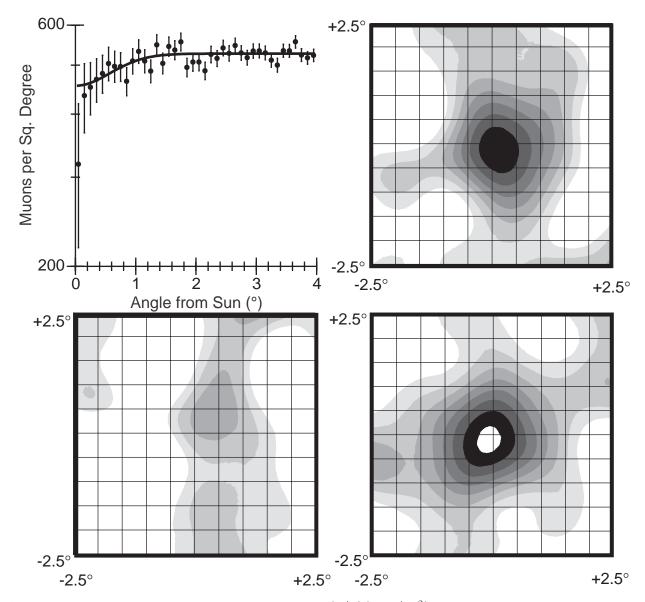Parker, E.N., 1963 *Interplanetary Dynamical Processes*, Interscience, New York.

Figure 1: (a) (upper left) The angular density of muons, $(1/\pi)(dN_\mu/d\theta^2)$ vs. θ, the angular distance between the muon direction and the calculated position of the center of the sun. The line is a fit to the data using Eq. 1. (b) (upper right) Contour map of the normalized deviations, Z, for a $\pm 2.5° \times \pm 2.5°$ region centered on the sun with a rebinning kernel $\sigma_k = 0.59°$. The contour lines are spaced by $\Delta Z = 0.5$ and are shown only where $Z \leq 0.0$. (c) (lower left) Same as (b) for the years 1989 to 1994. (d) (lower right) Same as (b) for the years 1995 to 1998, except that the unshaded region in the center of the plot indicates $-4.5 < Z < -4.0$.